Long- and short-term dynamic stability of submarine slopes undergoing hydrate dissociation

Xiaolong Song[1,2a], Tingkai Nian*[1b], Thomas Mestdagh[3c]; Marc De Batist*[2d]

1. State Key Laboratory of Coastal and Offshore Engineering, Dalian University of Technology, Dalian, Liaoning, 116024, China

2. Renard Centre of Marine Geology, Department of Geology, Ghent University, Krijgslaan 281 (S8), 9000 Ghent, Belgium

3. Flanders Marine Institute, InnovOcean site, Wandelaarkaai 7, 8400 Oostende, Belgium

---

*Corresponding author, Tingkai Nian, Email: tknian@dlut.edu.cn

Co-corresponding author, Marc De Batist, Email: marc.debatist@ugent.be

a Ph.D. Student, Email: songxiaolong@mail.dlut.edu.cn

b Ph.D., Professor, Email: tknian@dlut.edu.cn

c. Ph.D., Researcher, Email: thomas.mestdagh@vliz.be

d. Ph.D., Professor, Email: marc.debatist@ugent.be

Abstract

Natural gas hydrates (NGHs) have recently been recognized as a promising source of relatively clean alternative energy and a significant factor in triggering marine geohazards. This paper presents a numerical method for calculating the transient excess pore pressure associated with hydrate dissociation in submarine sediments with THC (Thermo-Hydro-Chemical) coupling. Then, the dynamic stability of submarine slopes experiencing gas hydrate dissociation is evaluated based on limit equilibrium analysis considering the real evolution of excess pore pressure. Finally, this work is applied to investigate the dynamic responses of typical hydrate slopes in the Shenhu Sea area, South China Sea (SCS), under two different timescales: 1) Case I: gradual temperature increases at the seafloor due to climate warming and 2) Case II: sharp temperature increases in the interior of the hydrate deposit due to hydrate extraction. In Case I, the timescale of hydrate dissociation is millennial. Due to the long-term temperature rise, the hydrate will dissociate slowly, which allows the generated free gas to migrate upwards and gradually accumulate at the transition zone between a porous layer and an overlying low-permeability layer. Eventually, the slow accumulation of free gas may lead to disc-shaped failure of the hydrate-bearing slope. In contrast, in Case II, the temperature rises sharply over a short period of time, which leads to the drastic dissociation of the hydrate. The timescale of hydrate dissociation is decadal. As a result, the excess pore pressure accumulates rapidly. Under the influence of excess pore pressure, the sediment will deform dramatically, which may cause a penetration failure of the hydrate-bearing slope. These findings are relevant to the long-term (millennial) safety of human beings and short-term (decadal) utilization of energy resources.

Keywords: Marine gas hydrate dissociation; THC coupling analysis, Dynamic stability; Slope failure

pattern, Shenhu area.

1. Introduction

Natural gas hydrates (NGHs) are cage-shaped crystalline compounds formed under low temperature and high pressure. Approximately 97% of the known hydrate reserves are found in marine sediments (Boswell and Collett, 2006). They are characterized by large volumes and high energy density, making them a promising alternative energy source. A hydrate reservoir forms a dynamically stable system under certain thermal, hydrological, and chemical (THC) states. The dissociation of hydrates can release large amounts of gas. If the total volume of the product is greater than the volume of the hydrate consumed, the local pore pressure will increase abnormally. This will lead to local sediment failure, which may gradually develop into a large-scale failure, leading to landslides (Deng et al., 2020a and 2020b). Both in situ observations and numerical simulations indicate that human activities (Ye et al., 2022) and climate warming (Ketzer et al., 2020) can cause the dissociation of hydrates in submarine strata (Fig. 1), which may lead to catastrophic geological hazards, such as submarine landslides. For instance, hydrate dissociation may have promoted (or facilitated) the triggering of the Storegga Slide (Sultan et al., 2004), the Slipstream Slide (Yelisetti et al., 2014), and the Tuaheni Landslide Complex (Mountjoy et al., 2015) and may furthermore endanger the seafloor ecological environment and offshore installations (Vanneste et al., 2014, Nian et al., 2018, Guo et al., 2021 and 2022a). According to the latest research, the cohesion of methane hydrate in marine sediments is significantly less than previously supposed, which makes slopes more vulnerable to internal and external factors (Atig et al., 2020). Therefore, it is important to improve our understanding of the long-term and short-term dynamic responses of submarine slopes undergoing hydrate dissociation.

Fig. 1. Schematic representation of the response of hydrate deposits to a temperature rise. Thermal stimulation of hydrates during extraction and/or climate warming caused by greenhouse gas emissions will shift the initial geothermal profile by ΔT on different timescales. As a result, hydrates will dissociate in the substratum.

At present, it is widely acknowledged that the accumulation of excess pore pressure in a submarine slope undergoing hydrate dissociation may trigger failure (even in gentle slopes), as obtained through geological exploration (Li et al., 2016; Gullapalli et al., 2019), physical modelling (Zhang et al., 2015; Nian et al., 2022), and numerical simulation (Jiang et al., 2015; Zhang et al., 2019). In recent years, the calculation model of excess pore pressure associated with hydrate dissociation has been investigated. For instance, Nixon and Grozic (2007) quantified the excess pore pressure resulting from hydrate dissociation under undrained conditions by setting a given amount of dissociation. Xiong and Zhang (2012) refined this model by considering the solubility of methane, while Zhang et al. (2019) included the compressibility factor of natural gas in this model. Chen et al. (2020) accounted for the equilibrium pressure and temperature of hydrates during dissociation in this model, in line with similar studies by Liu et al. (2010), Grozic (2010), and Zhu and Jia (2020). However, the pore pressure models incorporated in these studies cannot capture the temporal evolution of excess pore pressure due to the absence of THC coupling analysis, so they also cannot predict the dynamic response of hydrate-bearing slopes and accurately evaluate slope stability.

In this paper, a relatively simple but practical numerical method is presented to calculate the hydrate-associated excess pore pressure (coupling THC analyses) and evaluate the temporal evolution of the hydrate-bearing slope stability/instability through the developed code. A one-dimensional slope model is built by integrating Xu and Ruppel's (1999) work on THC-coupled analysis and Nixon and

Grozic's (2007) nonescape theory for pore fluids to compute the transient pore pressure caused by gas hydrate dissociation. This paper opted for a 1D model because most hydrates occur in stratigraphically constrained reservoirs that lack significant lateral variations (Archer et al., 2009). Based on the limit equilibrium method, the transient excess pore pressure is used to evaluate the dynamic stability of the hydrate slope. A MATLAB code is developed to realize this method. This method allows us to simulate the dynamic evolution of hydrate reservoirs and investigate the dynamic response of submarine slopes undergoing hydrate dissociation on different timescales, i.e., the long term (millennial) and short term (decadal). First, the Shenhu area (South China Sea) is selected as the research area due to the complex geological environment and the occurrence of large hydrate reserves. A typical hydrate-bearing slope in this area is chosen as a subject. This typical submarine hydrate-bearing slope is simplified into a geological model that comprises three layers of sediment (hydrate-bearing layer, impermeable overburden, and underburden) based on logging and seismic data. Then, two possible conditions are set up to describe the long-term and short-term effects on the hydrate reservoir: 1) gradual temperature increases at the seafloor due to climate warming and 2) sharp temperature increases within the hydrate deposit due to hydrate extraction. With this method, the dynamic response of the temperature profile, hydrate saturation profile, accumulation of excess pore pressure, and slope stability under these two different timescales are discussed. Finally, based on these experimental results and geological evidence, this study evaluates the possible failure patterns of the slope under these two cases.

2. Geological setting

This paper focuses on the Shenhu area, which is located in the centre of the northern continental slope of the South China Sea (Fig. 2) and is a major target area for commercial gas production. The

Guangzhou Marine Geological Survey (GMGS) conducted comprehensive geological surveys in the Shenhu area in 2007 and 2015 (Guo et al., 2017, Zhan et al., 2022). The specific drilling areas are shown in Fig. 2. Seismic data show a widely distributed bottom simulating reflector (BSR) in this area, characterized by strong reflection events roughly parallel to the seabed, indicating the existence of hydrate layers parallel to the seabed. Another distinctive feature of the region is the presence of 19 downslope-extending submarine canyons. Numerous small-scale submarine landslides are identified in association with these canyons; specifically, a total of 77 landslides are defined, including 61 individual slumps and 16 landslide complexes that consist of two or more component landslides (He et al., 2014). These slides are prone to slide again in the presence of external disturbances (Nian et al., 2019).

Fig. 2. Location of seismic line A-A′, site W19, GMGS1 drilling area, and GMGS3 drilling area in the Shenhu area, South China Sea (modified from Zhang et al., 2018).

A typical slope with a high hydrate saturation at site W19 (GMGS3) in the Shenhu area is considered in this paper (see Fig. 3a). The location of this site is shown in Fig. 2. The water depth at this site is 1274 m, and the drilling depth is 243 m below the seafloor. From the seismic profile over site W19 (see Fig. 3a), it can be seen that there are significant fluid migration channels under the BSR, forming columnar features with chaotic reflections and fuzzy or even blanked zones, which have been interpreted as gas chimneys (Zhang et al., 2017). This indicates that there is a large amount of gas in this area, which provides a sufficient gas supply for the formation of high-saturation hydrate deposits. During logging while drilling (LWD), the response characteristics of reservoirs with high hydrate saturation were observed on the logging curves, including high resistivity (RES), high acoustic velocity, low acoustic time difference (DT), low apparent density (RHON), and low gamma ray (GR) (see Fig. 3b). The resistivity at 134-202 m below the sea floor (mbsf) shows a significant anomaly, and the total thickness of the anomaly is approximately 68 m; in this interval, a high-saturation hydrate deposit was found. The lithologic analysis of cores shows that the reservoir sediments are mainly fine-grained, with an average effective porosity of 0.3, an average hydrate saturation of 46.2%, and an average permeability of 5.50×10^{-15} m^2.

Fig. 3. (a) Seismic reflection profile interpretation of line A-A′ in the Shenhu area (location in Fig. 2) and (b) logging response at site W19 on seismic line A-A′. (modified from Zhang et al., 2017).

3. Methodology

3.1 Slope model and destabilization scenarios

The submarine hydrate-bearing slope described above is simplified into a geological model that comprises three layers of sediment with a slope angle of 3° (see Fig. 4). The hydrate layer is located in the interior of the formation and is bounded by impermeable overburden and underburden. The sediment layer is homogeneous along the direction parallel to the seafloor with uniform physical properties such as porosity, permeability, cohesion and friction angle. In this paper, two cases are considered to simulate the possible long-term and short-term effects on the hydrate reservoir. Case I represents a gradual temperature increase at the seafloor (z=0 mbsf) due to contemporary climate warming. The Earth's climate system has undergone significant changes in the last century due to the influence of human activities (Kretschmer et al., 2015). Observational records show that in addition to the atmosphere, the global ocean is also subject to a warming trend (IPCC, 2018). Both in situ investigations (Ketzer et al., 2020) and numerical simulations (Strenne et al., 2016) show that ocean warming related to climate change may cause the dissociation of gas hydrate deposits. As one of the most sensitive regions to global warming, the South China Sea could be especially vulnerable to this impact. According to previous research, the temperature in the China Seas experienced continuous warming between 1982 and 1997, with a warming trend of 0.23 K/decade (Li et al., 2021). Therefore, it is of great practical significance to study the long-term dynamic stability of natural gas hydrate-bearing slopes under anthropogenic climate warming. Specifically, a seafloor temperature rise at a rate of 0.025 K per year is considered, in line with the presently observed level of warming (IPCC, 2018). Case II represents a sharp temperature increase in the interior of the hydrate deposit (z=170 mbsf) due to gas extraction using the thermal stimulation method. The principle of the thermal stimulation method is to raise the temperature within the hydrate reservoir beyond the phase equilibrium temperature, which causes the hydrate to dissociate. The advantage of this method is that it allows effective control of the rate of hydrate exploitation. As the main target area for gas production, the Shenhu area has been successfully exploited twice in natural gas production tests in 2017 and 2020 (Wang et al., 2018, Ye et al., 2020). However, given the complex geological environment and the low strength of marine sediments in this area, the exploitation of hydrates in relation to slope instability should be considered (Tan et al., 2021, Guo et al., 2022b). Therefore, it is necessary to further understand the impact of hydrate dissociation on marine strata to provide a reference for engineering site risk assessment and commercial production of gas hydrates. By investigating the current exploitation test using heat injection (Tabatabaie et al., 2009), in the considered simulation, the temperature in the interior of the hydrate reservoir increases at a rate of 1.0 K per day over a period of 30 days due to gas extraction using the thermal stimulation method, and the elevated temperature is maintained thereafter.

Fig. 4. Schematic diagram of the simplified hydrate-bearing slope at site W19, and the position at which the temperature change is applied in the two considered cases: Case I: ΔT=0.025 K/yr at z=0 mbsf; Case II: 1.0 K/d at z=170 mbsf.

3.2 Numerical method

This paper attempts to establish a relatively simple but practical numerical method to evaluate the dynamic stability of submarine slopes during hydrate dissociation. By improving the existing THC model, this section describes the relationship between hydrate saturation evolution and transient excess pore pressure considering multifield coupling and applies it to the dynamic stability evaluation of submarine hydrate-bearing slopes. The method is run in MATLAB through the developed code. An overview of the whole calculation process is given in Fig. 5. The different calculation steps in this method are explained below. Table 1 summarizes the values for the parameters adopted in the present study.

Fig. 5. A flowchart of the research work in this study.

Table 1. Summary of parameters and units used in this study.

3.2.1. Excess pore pressure accumulation coupling THC analysis

First, the THC coupling model of Xu and Ruppel (1999) is adopted to define the initial conditions for marine hydrate reservoirs. This model provides a series of equations to determine the positions of the top and bottom of the hydrate deposit zone (HZ) and the initial hydrate saturation profile throughout the HZ by solving one-dimensional mass, energy, and methane balance equations based on THC coupling. These equations are controlled by in situ pressures and temperatures, the fluxes of total mass (q_f), the fluxes of energy (q_e), the flux of methane (q_m), and the solubility of methane gas in the liquid phase (M_{sl}), which is a function of temperature and pressure and can be derived from Davie et al. (2004). The authors note that the formation and stability of hydrates requires not only appropriate temperature and pressure conditions but also an adequate supply of methane, which means that the availability of methane in the pore water must be equal to or exceed its solubility.

Second, the response of the above established configuration to an imposed change in temperature is modelled. The temporal evolution of the subsurface temperature profile through time *t* and space *z* towards a new equilibrium situation can be described by the one-dimensional heat conduction equation (Mestdagh et al., 2017):

$$\frac{\partial T(z,t)}{\partial t} = \kappa \frac{\partial^2 T}{\partial z^2} + s(z,t) \qquad (1)$$

where $s(z, t)$ is a term accounting for possible heat sources/sinks and κ is the effective thermal diffusivity (in m^2/s), which is proportional to the effective thermal conductivity. Then, Eq. (1) is numerically solved using the finite difference method,

$$T_{i,\ j} = T_{i\text{-}1,\ j} + \frac{\kappa \Delta t}{\Delta z^2}(T_{i\text{-}1,\ j\text{-}1} - 2T_{i\text{-}1,\ j} + T_{i\text{-}1,\ j+1}) \qquad (2)$$

where $T_{i,j}$ is the temperature at depth j and time i, which can be calculated based on the temperature at depths j, j-1, and j+1 in the previous time step i-1. Δt and Δz represent the time step and depth step, respectively, and are bound to the condition $\Delta t \le \frac{\Delta z^2}{2\kappa}$ for the numerical solution to be stable. Eq. (2) is solved using the following boundary conditions: (1) At t=0, the initial temperature at depth z is defined using the THC model of Xu and Ruppel (1999). (2) The temperature evolution through time at the top boundary, i.e., the seafloor, is prescribed by the considered climate change scenario (case I) or thermal stimulation path (case II).

Third, the change in the subsurface temperature and pressure state will disturb the stability of the hydrate reservoir and cause it to dissociate, which involves a phase transition and thus consumes latent heat. To account for the consumption of latent heat, the heat integration method is adopted, in line with Mestdagh et al. (2017). The temperature at each depth step ($T_{i,\ j}$) is first compared with the phase equilibrium temperature of the hydrate at that depth ($T_{diss,\ j}$), which is derived from CSMHYD (Sloan, 1998). When $T_{i,\ j}$ exceeds $T_{diss,\ j}$, hydrates start to dissociate. During the phase transition, heat is added while the temperature remains constant at T_{diss}. To dissociate all hydrate, the total amount of heat added needs to exceed the latent heat of the gas hydrate L_h. Only after all the hydrates have been dissociated can the temperature resume rising. The hydrate saturation S_h (i.e., the volume fraction of the pore space occupied by hydrate) at time i and depth j and the change in hydrate saturation over time can be described as follows:

$$S_{hi,\ j} = S_{h\,j} \times \frac{L_h - \Sigma dQ_{i,\ j}}{L_h} \qquad (3)$$

$$\Delta S_{hi,\ j} = \Sigma(S_{hi,\ j} - S_{hi\text{-}1,\ j}) \qquad (4)$$

where $S_{h\,j}$ represents the initial hydrate saturation at depth z_j; $\sum dQ_{i,\ j}$ denotes the total heat that has accumulated since the start of hydrate dissociation to time t_i, with $dQ_{i,\ j}$ calculated as $C_p \cdot (T_i - T_{i-1})$, in which C_p denotes the effective isobaric specific heat capacity; and $\Delta S_{hi,\ j}$ is the cumulative change in hydrate saturation (and thus representative of the amount of hydrate dissociation).

Finally, the excess pore pressure can be calculated using the above established parameters. For simplicity, the following assumptions are made, in line with earlier work (Nixon and Grozic, 2007; Zhang et al., 2019): (1) the sediments are dominantly fine-grained, so the permeability is very low; (2) the methane in the pore water is saturated, and the solubility of free gas generated by hydrate dissociation in the water is ignored; and (3) the sediment particles, hydrates and water are incompressible. Based on these assumptions, the volume changes in hydrate-bearing sediments are equal to the volume of gas produced by hydrate dissociation. The decrease in effective stress is related to the expanded volume and the excess pore pressure generated under hydrate dissociation (Terzaghi et al., 1943):

$$u_e = -E_s \Delta \varepsilon_v \qquad (5)$$

where u_e is the excess pore pressure caused by hydrate dissociation, E_s is the confined compression modulus, which can be obtained by field or laboratory tests, and $\Delta\varepsilon_v$ is the volume strain caused by u_e, given by:

$$\Delta \varepsilon_v = -\frac{\Delta V}{V} = -\phi \Delta S_h (V_g + V_{wh} - 1) = -\phi \Delta S_h \left(\frac{164.6 p_{atm} T_{nat}}{T_{atm} p_{nat}} + V_{wh} - 1\right) \qquad (6)$$

where ΔV and V are the volume increase and total volume of hydrate-bearing sediments, respectively; ϕ is the porosity of the sediments; ΔS_h is the amount of hydrate dissociation, which can be calculated by Eq. (4); V_g and V_{wh} represent the volume of gas and water produced after the hydrate is completely dissociated; (V_g+V_{wh}-1) represents the volume increase generated by the dissociation of one volume of hydrate; p and T indicate pressure and temperature under different states, respectively; and the subscripts atm and nat represent the standard state and the real state, respectively. The combination of Equations (4), (5), and (6) allows the transient excess pore pressure during hydrate dissociation to be obtained. It should be noted that since the dissipation of pore pressure is not considered in this paper, the excess pore pressure obtained here is overestimated, which yields a conservative result and conducive to slope safety evaluation.

3.2.2. Limit equilibrium stability analysis of submarine hydrate-bearing slopes

The limit equilibrium method (LEM) based on the infinite slope sliding mode is widely used to evaluate the stability of submarine slopes, especially for infinite slopes whose longitudinal dimension is much larger than their thickness (Liu et al., 2020; Guan et al., 2021). Geological surveys show that the typical distribution mode of hydrate layers in the Shenhu area is parallel to the sea bed, with an impermeable overburden of a certain thickness (Wang et al., 2018). Therefore, a simplified three-layer sediment model is adopted. The direction of the force system is shown in Fig. 6. From the perspective of the limit equilibrium analysis, the safety factor of the slope (Fs) is the ratio of the resistance shear force to the driving shear force acting on the slide plane, given by:

$$Fs == \frac{\int \bar{\tau}_{r} dl}{\int \bar{\tau}_{d} dl} = \frac{c' + \sigma_0' \tan\varphi'}{\tau_d} \quad (7)$$

where $\bar{\tau}_r$ and $\bar{\tau}_d$ are the shear resistance and driving force, respectively, acting on the unit slide plane dl; c' is the effective cohesion, which varies with the dissociation of hydrate; φ' is the internal friction angle; and σ_0' is the effective overburden stress, which can be obtained by subtracting the excess pore pressure u_e (obtained via Eq. (5)) from the initial overburden stress σ (equal to $\gamma' H cos2\alpha$, in which γ' is the buoyant unit weight of the sediments and H refers to the depth of the sliding plane). The driving force (τ_d) acting on the unit element can be written as follows:

$$\tau_d = \gamma' H \sin\alpha \cos\alpha \quad (8)$$

In addition, σ_a' and τ_a are the normal stress and shear stress acting on the lateral side of the unit element, respectively, which do not affect the stability analysis. Substituting Eq. (8) into Eq. (7) yields the expressions for the safety factor Fs:

$$F_s = \frac{c'}{\gamma' H \sin\alpha \cos\alpha} + \left(1 - \frac{u_e}{\sigma}\right) \frac{\tan\varphi'}{\tan\alpha} \quad (9)$$

Eq. (9) indicates that the dissociation of hydrate affects the stability of the slope from two aspects.

One is that the dissociation of hydrate will reduce the shear strength of sediment due to the disappearance of the cementation between sediment particles (the first term on the right side of Eq. (9)); the other is that the excess pore pressure generated by the dissociation of hydrate will significantly reduce the effective stress of the stratum and destabilize the slope (the second term on the right side of Eq. (9)). This is also in line with the common understanding of many scholars (Zhang et al., 2019; Liu et al., 2020). In Section 3.2.1, we obtained the excess pore pressure considering THC coupling under the condition of hydrate dissociation. In this paper, it is assumed that the cohesion of the hydrate-bearing sediments linearly decreases from 100 kPa to 5.5 kPa as the hydrate dissociates, according to Luo et al. (2016)'s triaxial compression test results. It is noted that other models of cohesion reduction due to hydrate dissociation can also be easily integrated in this method.

Fig. 6. (a) Schematic diagram of an infinite submarine slope undergoing hydrate dissociation. (b) The force system acting on the unit slide plane. Note: For illustration, the position of the slide plane in this figure is assumed, and its real position will change with the propagation of the dissociation front of the hydrate reservoir.

3.2.3. **Validation**

To validate the presented method for simulating transient pore pressure during hydrate dissociation, two cases simulated by Reagan and Moridis (2008) with TOUGH+HYDRATE for investigating the dynamic response of oceanic hydrate deposits to temperature change are replicated. Case I represents a typical scenario of shallow, cold hydrate deposits at 320 m water depth, with a temperature at the sea floor (T_0) of 0.4°C and geothermal gradient of 3°C/100 m, representative of conditions on Arctic continental margins. Case II describes a shallow, warmer hydrate deposit at 570 m water depth, T_0=6°C, and a geothermal gradient of 2.8°C/100 m. This case is representative of the upper continental slopes of the Gulf of Mexico. For both cases, a hypothetical temperature increase at an annual rate of 0.03°C over 100 years is imposed on the seafloor. The boundary and initial conditions are duplicated in this study and reflect the parameters reported in Reagan and Moridis (2008).

Fig. 7. The evolution of hydrate saturation profiles: (a) Case I: cold, shallow hydrate deposits; (b) Case II: warm, shallow hydrate deposits.

Fig. 7 shows that the results obtained with the model in this study are in good agreement with the findings of Reagan and Moridis (2008). In both cases, hydrates start to dissociate at the top and base of the reservoir as temperatures begin to increase. This is because the hydrates at the bottom of the reservoir are more sensitive to temperature increases, and even a slight downward heat flux is sufficient to trigger dissociation. Because of the steady heat source at the seafloor, the hydrate dissociation at the top of the reservoir is more dramatic, (i.e., a quicker downward propagation of the dissociation front). It should be noted that case II describes a shallow, warmer hydrate deposit. The geothermal profile is higher than that in case I. Therefore, the hydrate in case II is more sensitive. In addition, the hydrate reservoir in case 2 is shallower and closer to the heat source. Due to the above two reasons, the hydrate in case 2 decomposed rapidly, and the saturation became 0 at 100 years. These hydrate profiles clearly show stronger, rapid, and prominent responses at the top of the reservoir to temperature changes in seafloor temperature as the temperature increase propagates downwards.

4. Results and discussion

This section presents the results obtained by running the above model for the different scenarios outlined in Section 3.1. It evaluates the evolution of the subsurface temperature and hydrate saturation profile and the dynamic stability of the slope. In addition, the dynamic response of the slope at different timescales is discussed, and the failure mode of the slope is predicted based on these results.

4.1 Gradual temperature increase at the seafloor due to climate warming

4.1.1 Evolution of the hydrate reservoir

Fig. 8 illustrates the dynamic response of the hydrate reservoir to a gradual temperature increase at the seafloor due to climate warming (at a rate of 0.025 K per year over a period of 300 years). Fig. 8a shows the evolution of the subsurface temperature profile over a period of 20 kyr (kiloyears), where the dotted line represents the base of the theoretical hydrate stability zone (BHSZ) determined by the initial temperature/pressure profile (blue line) and the hydrate phase equilibrium curve (black line), whereas the dashed lines represent the top (THZ) and base (BHZ) of the initial, actual hydrate occurrence zone. The occurrence of hydrates is not only related to the temperature–pressure profile but also requires a continuous and sufficient supply of methane. Therefore, in many cases, the BHSZ and BHZ do not coincide, and the BHSZ is located at a significantly deeper position (as in Fig. 8a). Due to the increase in the seafloor temperature, heat is gradually transferred downwards in the sediment column, and the subsurface temperature throughout gradually increases. Once the temperature profile in the hydrate layer exceeds the phase equilibrium curve (black line), hydrates begin to dissociate. Since hydrate dissociation is endothermic, a certain amount of latent heat is consumed, resulting in a temperature propagation delay at the hydrate dissociation front, as shown in Fig. 8a (colour line). After all the hydrates are dissociated, the temperature profile gradually evolves towards a new (linear) equilibrium.

Fig. 8. Evolution of (a) the temperature profile, (b) the hydrate saturation profile, (c) the border and dissociation front of the hydrate zone (HZ), and (d) the excess pore pressure due to a gradual temperature increase at the

seafloor caused by climate warming (Case I).

Fig. 8b and 8c show the evolution of the hydrate saturation profile and the border and dissociation front of the hydrate zone (HZ) with increasing temperature. As the temperature rises, dissociation starts at the top of the reservoir after 3.1 kyr, and the dissociation front moves downwards over time. Dissociation also occurs at the bottom of the reservoir after 6.8 kyr, where the hydrates are more sensitive to temperature increases. In addition, excess pore pressure accumulates with the dissociation of hydrate, forming a downward-moving peak during hydrate dissociation (Fig. 8d).

4.1.2 Dynamic stability of the submarine hydrate-bearing slope

The dissociation of hydrates will greatly affect the stability of the submarine slope. This section investigates how the stability of the submarine slope varies under the conditions imposed in Case I. The dissociation front of the hydrate is considered the potential slide surface and varies with time, as shown in Fig. 8c. Fig. 9a shows the temporal evolution of the slope safety factor throughout the sediment column. It can be seen that in the initial state, the safety factor within the hydrate reservoir is significantly higher than that outside the reservoir, which is due to the cementation of hydrate strengthening the sediment. With the dissociation of hydrate, the slope safety factor at the top of the reservoir decreases rapidly as the slope reaches a critical state. This is because, on the one hand, the sediment strength decreases due to the loss of cementation; on the other hand, the excess pore pressure generated by hydrate dissociation reduces the effective stress of the formation. Fig. 9b presents the temporal evolution of the minimum safety factor ($F_{s,m}$) of the slope. It can be seen from this figure that the slope safety factor remains constant until 3.1 kyr, i.e., until the start of hydrate dissociation. With the excess pore pressure buildup and decementation in sediments caused by hydrate dissociation, the magnitude of $F_{s,m}$ drops gradually to 1 after 4.6 kyr, which indicates that the slope has reached a critical state (blue dotted line in Fig. 9b) and has become prone to failure.

Fig. 9. (a) Evolving profile of slope safety factor variation along depth. (b) The temporal evolution of the minimum factor of slope safety under a gradual temperature increase at the seafloor due to climate warming (Case I).

4.2 Sharp temperature increase inside the hydrate reservoir due to hydrate extraction

4.2.1 Evolution of the hydrate reservoir

Fig. 10 illustrates the dynamic response of the hydrate reservoir to a sharp temperature increase within the hydrate deposit due to hydrate extraction using the thermal stimulation method (at a rate of 1.0 K per day over 30 days). Fig. 10a shows the evolution of the subsurface temperature profile. With the temperature increasing in the interior of the hydrate reservoir, heat is transferred both upwards and downwards. Once the temperature in the hydrate layer exceeds the phase equilibrium curve (black line), hydrates begin to dissociate. Similar to case I, a certain amount of latent heat is consumed due to hydrate dissociation, and the phenomenon of temperature propagation delay is also observed in this case, as shown in Fig. 10a (colour line). Fig. 10b shows the evolution of the hydrate saturation profile with increasing temperature. Due to the rapid and large rise in temperature, the dissociation of hydrate under this scenario is more severe than in case I. As the temperature rises, dissociation starts at the interior of the reservoir after 20 d, and the dissociation front propagates both upwards and downwards over time. Hydrate dissociation is complete within 30 yr. Fig. 10c shows the evolution of the position of the dissociation front, with the red line representing the dissociation front and the black line representing the initial boundary of the hydrate reservoir. The dissociation front propagates more rapidly downwards (towards the base of the hydrate zone) than upwards (towards the top of the hydrate zone). Additionally, all hydrates are dissociated before dissociation from the top/base of the original hydrate zone can occur, indicating that the reaction in the interior of the hydrate reservoir is more intense due to the proximity to the heat source. In addition, Fig. 10d shows the evolution curve of excess pore pressure. A peak is formed in the middle of the hydrate reservoir and expands up and down as the hydrate dissociates.

Fig. 10. Evolution of (a) the temperature profile, (b) the hydrate saturation profile, (c) the border and dissociation front of the hydrate zone (HZ), and (d) the excess pore pressure due to a sharp temperature increase inside the hydrate deposit caused by thermal stimulation during hydrate extraction (case II).

4.2.2 Dynamic stability of the submarine hydrate-bearing slope

This section investigates how the stability of the submarine slope will vary under the conditions imposed in Case II. Fig. 11a shows the temporal evolution of the slope safety factor with depth. Compared to Case I, the safety factor curve in the initial state is basically the same. With the dissociation of hydrate, the slope safety factor in the middle of the hydrate reservoir decreases rapidly as the slope reaches a critical state. Fig. 11b presents the evolution of the minimum safety factor ($F_{s,m}$) of the slope. The factor of safety remains constant until hydrates start to dissociate. As the temperature increases, the hydrate begins to dissociate at t_1=20 d. Compared to Fig. 9 (case I), the safety factor decreases more rapidly. It takes just 60 d to reach a safety factor of 1 at 80 d; at this point, the slope has reached a critical state.

Fig. 11. Temporal evolution of the slope safety factor (a) and the minimum factor of slope safety (b) under a sharp temperature increase inside the hydrate deposit due to hydrate extraction (case II).

4.3 Discussion

To intuitively explore the failure modes after slope instability at two different timescales, an experimental system is designed (Nian et al., 2022). Submarine slope failure triggered by overpressure free gas associated with gas hydrate dissociation is investigated in laboratory experiments. After the comprehensive consideration of the rate of hydrate dissociation at different timescales, several experiments were carried out. Based on the results described above, the possible failure patterns of the slopes considered in Cases I and II are discussed in combination with the experimental studies.

For Case I, disc-shaped failure is observed (as shown in Fig. 12a). The effect of climate warming on the temperature of the seabed stratum is relatively slow. It can be seen from Fig. 8 and Fig. 9 that the response of hydrate reservoirs under this condition occurs on millennial timescales. Since the considered hydrate reservoir is relatively highly permeable, gas will migrate upwards through the hydrate layer under the action of excess pore pressure after hydrate dissociation. However, because the overlying layers are usually fine-grained sediments with low permeability, gas accumulates at the transition zone between the hydrate reservoir and the overburden (Nian et al., 2022). As described in other studies (Sun et al., 2018), the sealing effect of the overlying layer will produce great excess pore pressure and drive the gas to migrate laterally. Meanwhile, as the gas accumulates, the overlying layer deforms constantly, creating a dome on the seafloor. In addition, the increasing excess pore pressure will trigger the formation of hydraulic fractures at the rim of the dome. When the fractures reach the seafloor, gas bursts through the seabed, forming a penetrating seepage channel and gas plume on the seafloor. Such structures can damage the integrity of the sediments and lead to slope failure. This failure pattern has, for example, been suggested by Sun et al. (2018) to explain repeated Quaternary slope failures in the northern South China Sea (Fig. 12b) based on analysis of seismic profiles and multibeam bathymetric data. These slope failures are located in the central part of the northern South China Sea and lie very close to the study site in this paper. The strata in their study area consist of coarse-grained turbidites (porous reservoir layer) overlain by fine-grained, low-permeability sediments (seal layer). High-amplitude seismic anomalies indicate that there is a large amount of free gas in the formation. The migration of free gas from deep strata into porous strata has led to the development of overpressure in the coarse-grained layer, leading to the formation of a weak layer in the transition zone to the overlying low-permeability layers. The existence of weak layers reduces the shear strength of the formation and may act as a precursor for slope failure.

Fig. 12. (a) Disc-shaped failure: a possible hydrate-bearing slope failure pattern under a gradual temperature increase at the seafloor due to climate warming (Nian et al., 2022); (b) schematic illustration of a slope failure case in the northern South China Sea (Sun et al., 2018)

Fig. 13a shows a possible failure pattern (penetration failure) under a sharp temperature increase due to hydrate extraction. Compared to that in Case I, the response in Case II is more rapid due to the intervention of human activities; it can be seen from Fig. 10 and Fig. 11 that hydrates dissociate on decadal timescales, resulting in a rapid buildup of excess pore pressure. The reason for the rapid buildup of pore pressure is the rapid accumulation of gas over a short time, which, as shown in experiments (Nian et al., 2022), will lead to a more intense failure pattern. Hydraulic fractures may be generated inside the hydrate reservoir and form gas-rich cavities. According to the theory of material mechanics, a large amount of accumulated gas will make the overlying sediment layer deform violently and form a dome on the seafloor. As opposed to the dome in Case I, severe deformation will produce fractures at the top of the dome and continue to extend to the interior of the sediment. Once the crack is connected to a gas-rich cavity, the gas will erupt, and a connected gas leakage channel will be formed, which can be regarded as slope failure. To our knowledge, there are no reported slope failures caused by the dramatic dissociation of hydrates due to hydrate extraction. However, related geological surveys can provide some indirect evidence. For example, Zhang et al. (2017) found that hydrate dissociation induces a strong gas swelling phenomenon and forms cavities, as observed in cored sediment samples in the Shenhu area, South China Sea (Fig. 13b). In addition, when Paull et al. (2008) explored the association between the formation of seabed mounds and hydrate accumulation using an autonomous underwater vehicle (AUV), they found a mound with a tensile fracture near the crest of the mound from which gas continuously escaped, and gas-hydrate-containing bubbles were collected (Fig. 13c). Therefore, the mound was likely caused by the accumulation of gas generated by the dissociation of hydrates. The clues from these geological surveys provide support for the failure pattern proposed in this paper.

Fig. 13. (a) Penetration failure: a possible hydrate-bearing slope failure under a sharp temperature increase due to hydrate extraction (Nian et al., 2022); (b) cavity structure resulting from the dissociation of gas hydrate in the Shenhu area (Zhang et al., 2017); (c) a crack near the crest of a dome in the Santa Monica Basin, offshore California, from which a continuous plume of gas emanates (modified from Paull et al., 2008).

In addition, it can be seen from Section 4.1 that the impact of climate warming on a submarine hydrate-bearing slope is a long-term process and potentially has a wide lateral extent (since the temperature increase is likely to affect the slope as a whole). This may induce extensive dissociation of hydrates resulting in massive slope failure, as, for example, suggested for the Storegga slide, which covers an area of 85-90,000 km^2 (Sultan et al., 2004). Such a vast area may encompass variations in slope angle, as is also the case in the Shenhu Sea area, which features numerous submarine canyons. In contrast, for anthropogenic influences such as hydrate extraction, the effect on a slope is usually short in duration and more local (due to the very local temperature increase inside the hydrate reservoir). It is therefore reasonable to assume that the slope angle is constant over the affected area. However, hydrate extraction may cause local instability of the slope (Vanneste et al., 2014). More work (e.g., 2D/3D modelling) needs to be done to evaluate the influence of such variations in slope angle and lateral extent of the area affected by hydrate dissociation on the stability of a hydrate-bearing slope. Moreover, the thermal conductivity, permeability, saturation of the formation and cohesion of the sediments all affect the stability of the hydrate-bearing slope and its subsequent spatiotemporal evolution. The coupled relationships between these parameters and the triggering mechanisms for slope instability also need more in-depth research.

5. Conclusions

This paper studied the long-term (millennial) and short-term (decadal) dynamic stability of a submarine slope undergoing hydrate dissociation. Based on THC coupling, the transient excess pore pressure caused by hydrate dissociation is modelled through the developed code, and the dynamic stability of the slope is evaluated under two different timescales. The main conclusions are as follows:

1. The dynamic response of the highly saturated hydrate reservoir to a gradual temperature increase at the seafloor due to climate warming is investigated. Dissociation starts at the top of the reservoir after 3.1 kyr. With the dissociation of hydrates, the slope safety factor gradually decreased and reached the critical state after 4.6 kyr.

2. The present research also studies the dynamic response of this highly saturated reservoir to a sharp temperature increase inside the hydrate deposit due to hydrate extraction. In this case, heat is transferred both upwards and downwards from the point where the temperature rise is induced, and hydrate dissociation initiates. The hydrate began to dissociate after 20 days of heating, resulting in a decrease in the slope safety factor and reaching the critical state in 80 days.

3. Two distinct slope failure patterns are proposed for the two different simulations: (1) Disc-shaped failure: Under a long-term temperature rise, the hydrate dissociates slowly, and the free gas migrates upwards under the influence of excess pore pressure and gradually accumulates at the transition zone between the porous layer and the overlying low-permeability layer, eventually leading to slope failure. (2) Penetration failure: A short-term temperature rise causes hydrate dissociation, resulting in the accumulation of excess pore pressure. Under the influence of excess pore pressure, the sediment layer deforms violently and forms a penetrating fracture at the crest of the dome, which can be seen as a slope failure.

The research in this paper is of great significance to better understanding the multi-timescale dynamic response and related risk assessment of submarine hydrate reservoirs after external environmental/anthropogenic changes.

Acknowledgments

This research presented here was supported by the National Natural Science Foundation of China (No.52079020 & 42077272), the LiaoNing Revitalization Talents Program (No. XLYC2002036) and the China Scholarship Council (No. 201906060077). Their support is gratefully acknowledged.

6. References

Archer D, Buffett B, Brovkin V (2009) Ocean methane hydrates as a slow tipping point in the global carbon cycle. *Proceedings of the National Academy of Sciences of the United States of America* 106(49): 20596-20601.

Atig D, Broseta D, Pereira JM, Brown R (2020) Contactless probing of polycrystalline methane hydrate at pore scale suggests weaker tensile properties than thought. *Nature Communications* 11(1):3379.

Boswell R, Collett TS (2006) The Gas Hydrates Resource Pyramid, Fire in the Ice: Methane Hydrate 6(3):5-7.

Chen YM, Zhang LL, Liao CC, Jiang MJ, Peng M (2020) A two-stage probabilistic approach for the risk assessment of submarine landslides induced by gas hydrate exploitation. *Applied Ocean Research* 99:102158.

Davie MK, Zatsepina OY, Buffett BA (2004) Methane solubility in marine hydrate environments. *Marine Geology* 203(1-2):177-184.

Deng XJ, Pan SW, Zhang JB, Wang ZY, Jiang ZY (2020a) Numerical investigation on abnormally elevated pressure in laboratory-scale porous media caused by depressurized hydrate dissociation. *Fuel* 271:117679.

Deng XJ, Feng JW, Pan SW, Wang ZY, Zhang JB, Chen WQ (2020b) An improved model for the migration of fluids caused by hydrate dissociation in porous media. *Journal of Petroleum Science and Engineering* 188:106876.

Grozic JLH (2010) Interplay Between Gas Hydrates and Submarine Slope Failure. Submarine Mass Movements and Their Consequences - 4th International Symposium, Dordrecht, Springer Netherlands, pp:11-30.

Guan JA, Cong XR, Archer DE, Wan LH, Liang DQ (2021) Spatio-temporal evolution of stratigraphic-diffusive methane hydrate reservoirs since the Pliocene along Shenhu continental slope, northern South China sea. *Marine and Petroleum Geology* 125:104864.

Gullapalli S, Dewangan P, Kumar A, Dakara G, Mishra CK, Gas Hydrate Research Group (2019) Seismic evidence of free gas migration through the gas hydrate stability zone (GHSZ) and active methane seep in Krishna-Godavari offshore basin. *Marine and Petroleum Geology* 110:695-705.

Guo XS, Nian TK, Fan N, Jia YG (2021) Optimization design of a honeycomb-hole submarine pipeline under a hydrodynamic landslide impact. *Marine Georesources and Geotechnology* 39(9):1055-1070.

Guo XS, Nian TK, Stoesser T (2022a) Using dimpled-pipe surface to reduce submarine landslide impact forces on pipelines at different span heights. *Ocean Engineering* 244:110343.

Guo XS, Nian TK, Wang D, Gu ZD (2022b) Evaluation of undrained shear strength of surficial marine clays using ball penetration-based cfd modelling. *Acta Geotechnica* 17(5):1627-1643.

Guo YQ, Yang SX, Liang JQ et al. (2017) Characteristics of high gas hydrate distribution in the Shenhu area on the northern slope of the South China Sea. *Earth Science Frontiers* 24(4):24–31.

He Y, Zhong GF, Wang LL, Kuang ZG (2014) Characteristics and occurrence of submarine canyon-associated landslides in the middle of the northern continental slope, South China Sea. *Marine & Petroleum Geology* 57(2):546-560.

IPCC. (2018) Summary for policymakers. In: Masson-Delmotte V, Zhai P, Pörtner HO, Roberts D, Skea J, Shukla PR, Pirani A, Moufouma-Okia W, Péan C, Pidcock R, Connors S, Matthews JBR, Chen Y, Zhou X, Gomis MI, Lonnoy E, Maycock T, Tignor M, and Waterfield T. (Eds.) Global Warming of 1.5°C. an IPCC Special Report on the Impacts of Global Warming of 1.5°C above Pre-Industrial Levels and Related Global Greenhouse Gas Emission Pathways, in the Context of Strengthening the Global Response to the Threat of Climate Change, Sustainable Development, and Efforts to Eradicate Poverty. Geneva: World Meteorological Organization, pp:32

Jiang MJ, Sun C, Crosta GB, Zhang WC (2015) A study of submarine steep slope failures triggered by thermal dissociation of methane hydrates using a coupled CFD-DEM approach. *Engineering Geology* 190:1-16.

Ketzer M, Praeg D, Rodrigues LF, Augustin A, Pivel MAG, Rahmati-Abkenar M, Miller DJ, Viana AR, Cupertino

JA (2020) Gas hydrate dissociation linked to contemporary ocean warming in the southern hemisphere. *Nature Communications* 11(1):3788.

Kretschmer K, Biastoch A, Rüpke L, Burwicz E (2015) Modeling the fate of methane hydrates under global warming. *Global Biogeochemical Cycles* 29(5):610-625.

Li Y, Wang QY, Li QQ, Liu YW, Wang Y (2021) An asymmetric variation of hot and cold SST extremes in the China Seas during the recent warming hiatus period. *Scientific Reports* 11(1):2014.

Li A, Davies RJ, Yang JX (2016) Gas trapped below hydrate as a primer for submarine slope failures. *Marine Geology* 380:264-271.

Liu F, Tan L, Crosta G, Huang Y (2020) Spatiotemporal destabilization modes of upper continental slopes undergoing hydrate dissociation. *Engineering Geology* 264:105286.

Liu F, Wu SG, Sun YB (2010) A quantitative analysis for submarine slope instability of the northern South China Sea due to gas hydrate dissociation. *Chinese Journal of Geophysics*, 2010, 53(4): 93-98. (in Chinese)

Luo TT, Song YC, Zhu YM, Liu WG, Yu L, Li YH, Wu ZR (2016) Triaxial experiments on the mechanical properties of hydrate-bearing marine sediments of South China Sea. *Marine & Petroleum Geology* 77:507-514.

Mountjoy JJ, Pecher I, Henrys S, Crutchley G, Barnes PM, Plaza-Faverola A (2015). Shallow methane hydrate system controls ongoing, downslope sediment transport in a low-velocity active submarine landslide complex, Hikurangi Margin, New Zealand. *Geochemistry Geophysics Geosystems* 15(11):4137-4156.

Mestdagh T, Poort J, Batist MD (2017) The sensitivity of gas hydrate reservoirs to climate change: Perspectives from a new combined model for permafrost-related and marine settings. *Earth-Science Reviews* 169:104-131.

Nian TK, Guo X S, Fan N, Jiao H B, Li D Y (2018) Impact forces of submarine landslides on suspended pipelines considering the low-temperature environment. *Applied Ocean Research* 81:116-125.

Nian TK, Guo XS, Zheng DF, Xiu ZX, Jiang ZB (2019) Susceptibility assessment of regional submarine landslides triggered by seismic actions. *Applied Ocean Research* 93:101964.

Nian TK, Song XL, Zhao W, Jiao HB, Guo XS (2022) Submarine slope failure due to overpressure fluid associated with gas hydrate dissociation. *Environmental Geotechnics* 9(2):108-123.

Nixon MF, Grozic JLH. (2007) Submarine slope failure due to gas hydrate dissociation: a preliminary quantification. *Canadian Geotechnical Journal* 44(3):314-325.

Paull CK, Normark WR, Ussler W, Caress DW and Keaten R (2008) Association among active seafloor deformation, mound formation, and gas hydrate growth and accumulation within the seafloor of the Santa Monica Basin, offshore California. *Marine Geology* 250(3–4):258–275.

Reagan MT, Moridis GJ (2008) Dynamic response of oceanic hydrate deposits to ocean temperature change. *Journal of Geophysical Research: Oceans* 113(12).

Stranne C, O'Regan M, Dickens GR, Crill P, Miller C, Preto P Jakobsson M (2016) Dynamic simulations of potential methane release from East Siberian continental slope sediments. *Geochemistry, Geophysics, Geosystems* 17(3): 872-886.

Sultan N, Cochonat P, Foucher JP, Mienert J (2004) Effect of gas hydrate melting on seafloor slope instability. *Marine Geology* 213(1–4):379–401

Sun QL, Cartwright J, Xie XN, Lu XY, Yuan SQ, Chen CX (2018) Reconstruction of repeated Quaternary slope failures in the northern South China Sea. *Marine Geology* 401:17-35.

Tabatabaie SH, Darvish MP (2009) Analytical solution for gas production from hydrate reservoirs underlain with free gas. Journal of Natural Gas Science and Engineering 1(1–2): 46–57.

Tan L, Liu F, HuangY. Crosta G, Frattini P, Cen XQ (2021) Production-induced instability of a gentle submarine slope: Potential impact of gas hydrate exploitation with the huff-puff method. *Engineering Geology* 289:106174.

Terzaghi KT (1943) Theoretical Soil Mechanics. John Wiley & Sons New York.

Vanneste M, Sultan N, Garziglia S, Forsberg CF, L'Heureux JF (2014) Seafloor instabilities and sediment deformation processes: The need for integrated, multi-disciplinary investigations. *Marine Geology* 352:183-214.

Wang JL, Wu SG, Kong X, Li QP, Wang JX, Ding R (2018) Geophysical characterization of a fine-grained gas hydrate reservoir in the Shenhu area, northern South China Sea: Integration of seismic data and downhole logs. *Marine & Petroleum Geology* 99:895-903.

Xiong ZS, Zhang JH (2012) Effect of dissociation of gas hydrate on the stability of submarine slope. *31st ASME International Conference on Ocean, Offshore and Arctic Engineering*, Rio de Janeiro, Brazil, pp:95-101.

Xu WY, Ruppel C (1999) Predicting the occurrence, distribution, and evolution of methane gas hydrate in porous marine sediments. *Journal of Geophysical Research: Solid Earth* 104(B3):5081-5095.

Ye HY, Wu XZ, Li DY, Jiang YJ, Gong Bin (2022) A novel thermal stimulation approach for natural gas hydrate exploitation-the application of the self-entry energy compensation device in the Shenhu sea. *Journal of Natural Gas Science and Engineering* 105:104723.

Ye JL, Qin XW, Xie WW, Lu HL, Ma BJ，Qiu HJ, Liang JQ, Lu JA, Kuang ZG, Lu C, Liang QY, Wei SP, Yu YJ, Liu CS, Li B, Shen KX, Shi HX, Lu QP, Li J, Kou BB, Song G, Li B, Zhang HE, Lu HF, Ma C, Dong YF, Bian H (2020) Main progress of the second gas hydrate trial production in the South China Sea. *Geology in China* 47(3):557-568. (in Chinese with English abstract)

Yelisetti S, Spence GD, Riedel M (2014) Role of gas hydrates in slope failure on frontal ridge of northern Cascadia margin. *Geophysical Journal International* 199(1):441-458.

Zhan LS, Kang DJ, Lu HL, Lu JA (2022) Characterization of coexistence of gas hydrate and free gas using sonic logging data in the Shenhu Area, South China Sea. *Journal of Natural Gas Science and Engineering* 101:104540.

Zhang HT, Luo XQ, Bi JF, He GF, Guo ZJ (2019) Submarine slope stability analysis during natural gas hydrate dissociation. *Marine Georesources and Geotechnology* 37(4):467-476.

Zhang JH, Lin HL, Wang KZ (2015) Centrifuge modeling and analysis of submarine landslides triggered by elevated pore pressure. *Ocean Engineering* 109:419-429.

Zhang W, Liang JQ, Lu JA, Wei JG, Su PB, Fang YX, Guo YQ, Yang SX, Zhang GX (2017) Accumulation features and mechanisms of high saturation natural gas hydrate in Shenhu Area, northern South China Sea. *Petroleum Exploration and Development* 44(5): 670–679.

Zhang W, Liang JQ, Su PB, Wei JG, Sha ZB, Lin L, Liang J, Huang W (2018) Migrating pathways of hydrocarbons and their controlling effects associated with high saturation gas hydrate in Shenhu area, northern South China Sea. *Geology in China* 45(1):1-14. (in Chinese with English abstract)

Zhu CQ, Jia YG (2020) Submarine slope stability analysis during natural gas hydrate dissociation: Discussion. *Marine Georesources and Geotechnology* 38(6):753-754.

Figure captions

Fig. 1. Schematic representation of the response of hydrate deposits to a temperature rise. Thermal stimulation of hydrates during extraction and/or climate warming caused by greenhouse gas emissions will shift the initial geothermal profile by ΔT on different timescales. As a result, hydrates will dissociate in the substratum.

Fig. 2. Location of seismic line A-A′, site W19, GMGS1 drilling area, and GMGS3 drilling area in the Shenhu area, South China Sea (modified from Zhang et al., 2018).

Fig. 3. (a) Seismic reflection profile interpretation of line A-A′ in the Shenhu area (location in Fig. 2) and (b) logging response at site W19 on seismic line A-A′. (modified from Zhang et al., 2017).

Fig. 4. Schematic diagram of the simplified hydrate-bearing slope at site W19, and the position at which the temperature change is applied in the two considered cases: Case I: ΔT=0.025 K/yr at z=0 mbsf; Case II: 0.5 K/yr at z=170 mbsf.

Fig. 5. A flowchart of the research work in this study.

Fig. 6. (a) Schematic diagram of an infinite submarine slope undergoing hydrate dissociation. (b) The force system acting on the unit slide plane. Note: For illustration, the position of the slide plane in this figure is assumed, and its real position will change with the propagation of the dissociation front of the hydrate reservoir.

Fig. 7. The evolution of hydrate saturation profiles: (a) Case I: cold, shallow hydrate deposits; (b) Case II: warm, shallow hydrate deposits.

Fig. 8. Evolution of (a) the temperature profile, (b) the hydrate saturation profile, (c) the border and dissociation front of the hydrate zone (HZ), and (d) the excess pore pressure due to a gradual temperature increase at the seafloor caused by climate warming (Case I).

Fig. 9. (a) Evolving profile of slope safety factor variation along depth. (b) The temporal evolution of the minimum

factor of slope safety under a gradual temperature increase at the seafloor due to climate warming (Case I).

Fig. 10. Evolution of (a) the temperature profile, (b) the hydrate saturation profile, (c) the border and dissociation front of the hydrate zone (HZ), and (d) the excess pore pressure due to a sharp temperature increase inside the hydrate deposit caused by thermal stimulation during hydrate extraction (case II).

Fig. 11. Temporal evolution of the slope safety factor (a) and the minimum factor of slope safety (b) under a sharp temperature increase inside the hydrate deposit due to hydrate extraction (case II).

Fig. 12. (a) Disc-shaped failure: a possible hydrate-bearing slope failure pattern under a gradual temperature increase at the seafloor due to climate warming (Nian et al., 2022); (b) schematic illustration of a slope failure case in the northern South China Sea (Sun et al., 2018).

Fig. 13. (a) Penetration failure: a possible hydrate-bearing slope failure under a sharp temperature increase due to hydrate extraction (Nian et al., 2022); (b) cavity structure resulting from the dissociation of gas hydrate in the Shenhu area (Zhang et al., 2017); (c) a crack near the crest of a dome in the Santa Monica Basin, offshore California, from which a continuous plume of gas emanates (modified from Paull et al., 2008).

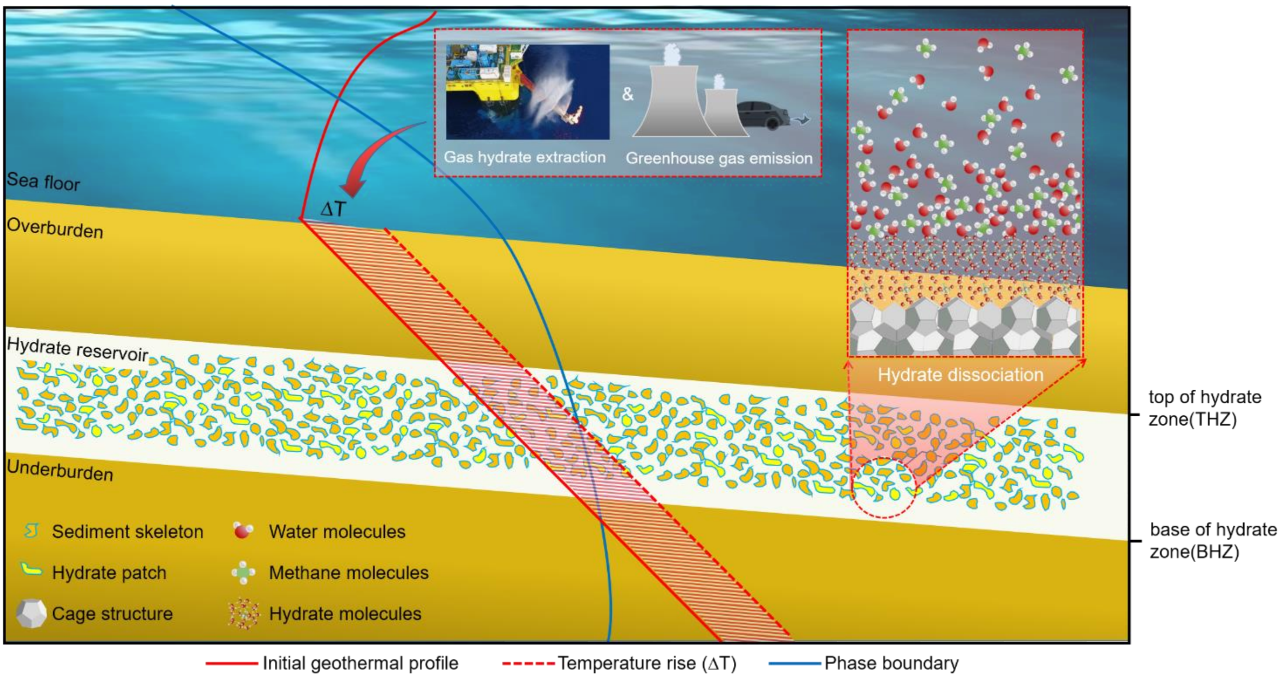

Fig. 1. Schematic representation of the response of hydrate deposits to a temperature rise. Thermal stimulation of hydrates during extraction and/or climate warming caused by greenhouse gas emissions will shift the initial geothermal profile by ΔT on different timescales. As a result, hydrates will dissociate in the substratum.

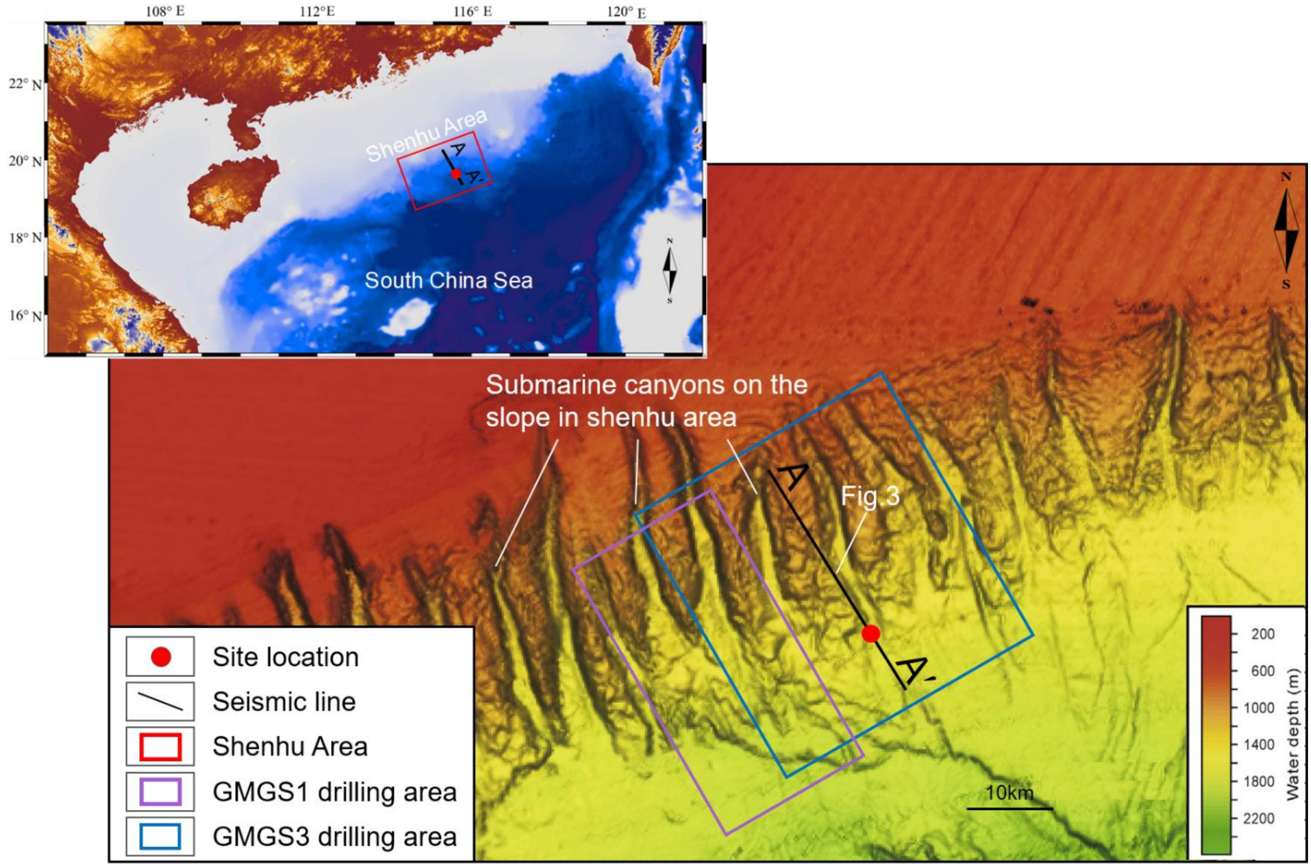

Fig. 2. Location of seismic line A-A′, site W19, GMGS1 drilling area, and GMGS3 drilling area in the Shenhu area, South China Sea (modified from Zhang et al., 2018).

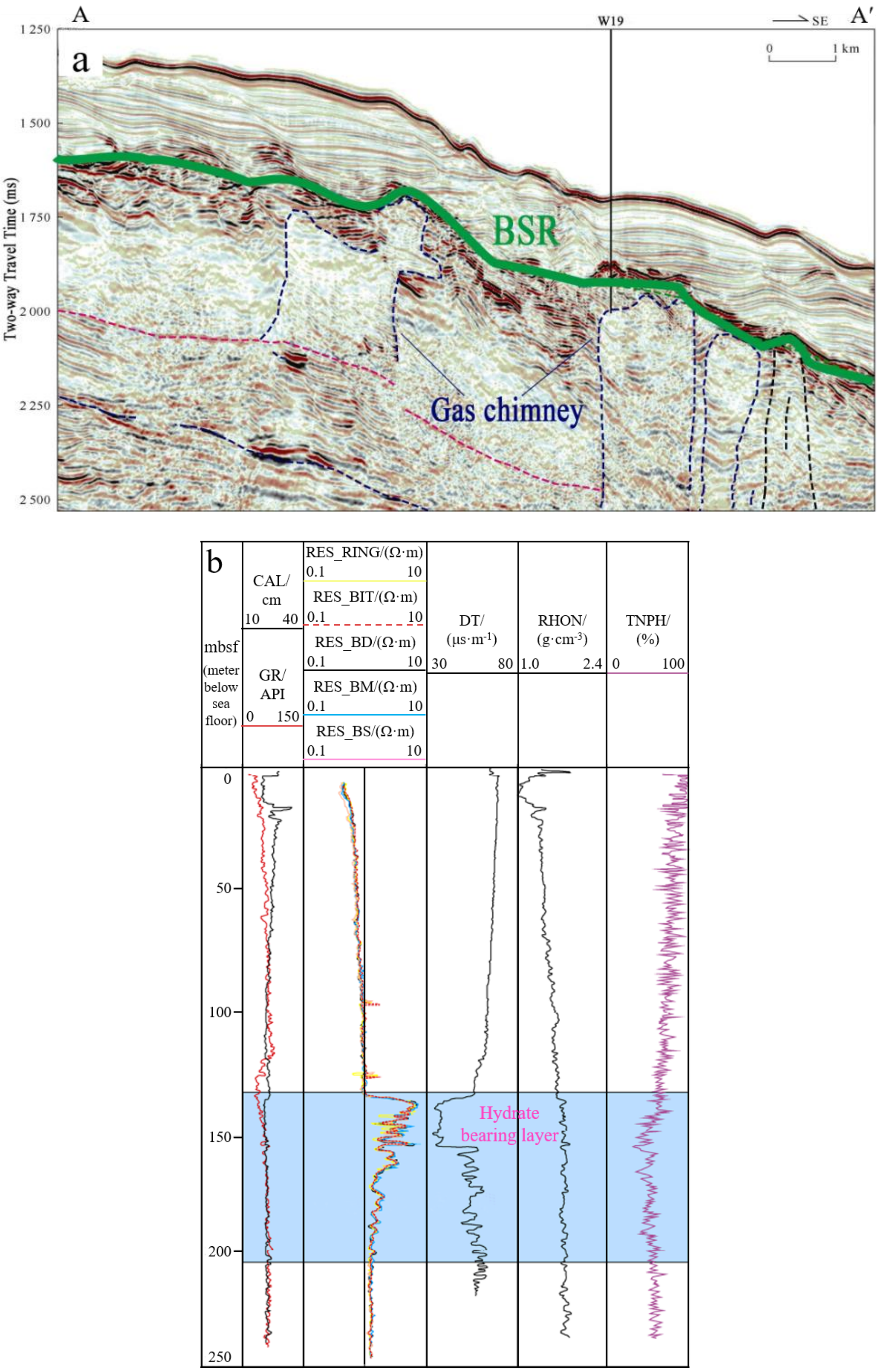

Fig. 3. (a) Seismic reflection profile interpretation of line A-A′ in the Shenhu area (location in Fig. 2) and (b) logging response at site W19 on seismic line A-A′. (modified from Zhang et al., 2017).

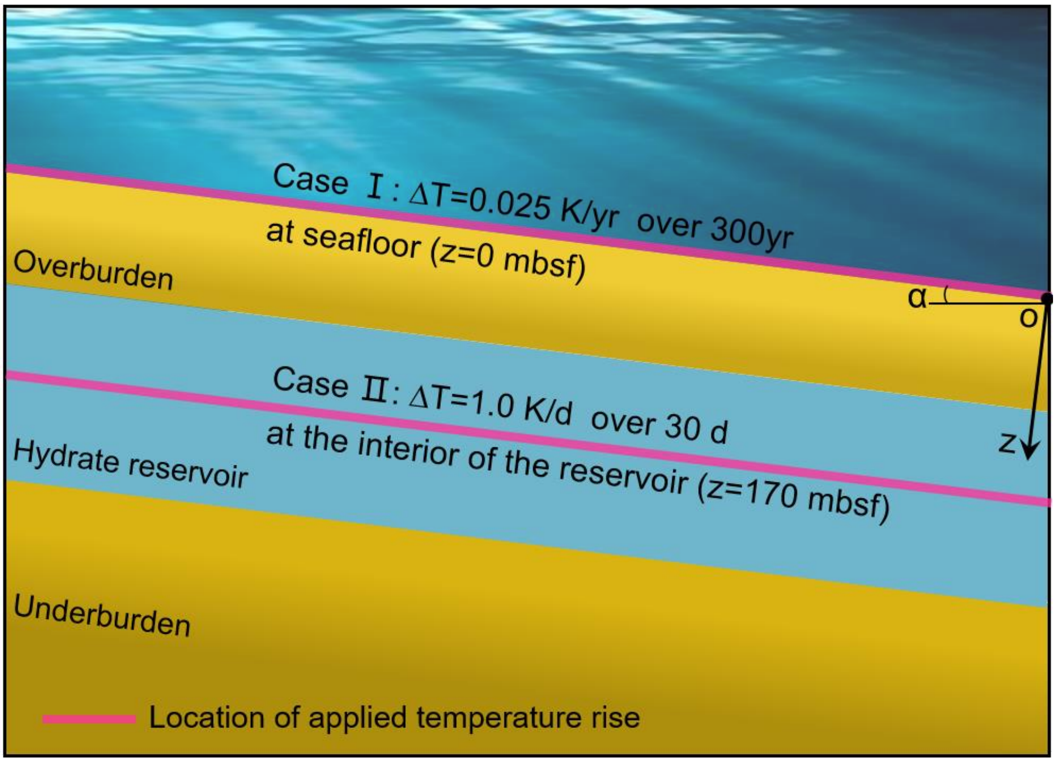

Fig. 4. Schematic diagram of the simplified hydrate-bearing slope at site W19, and the position at which the temperature change is applied in the two considered cases: Case I: ΔT=0.025 K/yr at z=0 mbsf; Case II: 0.5 K/yr at z=170 mbsf.

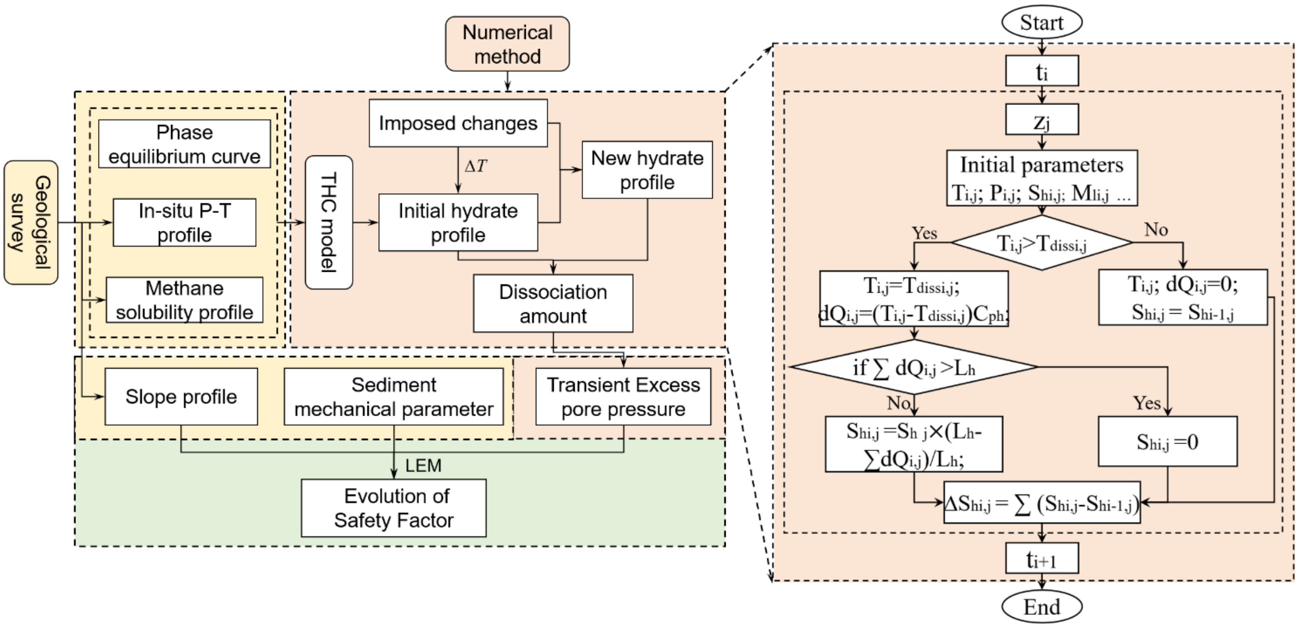

Fig. 5. A flowchart of the research work in this study.

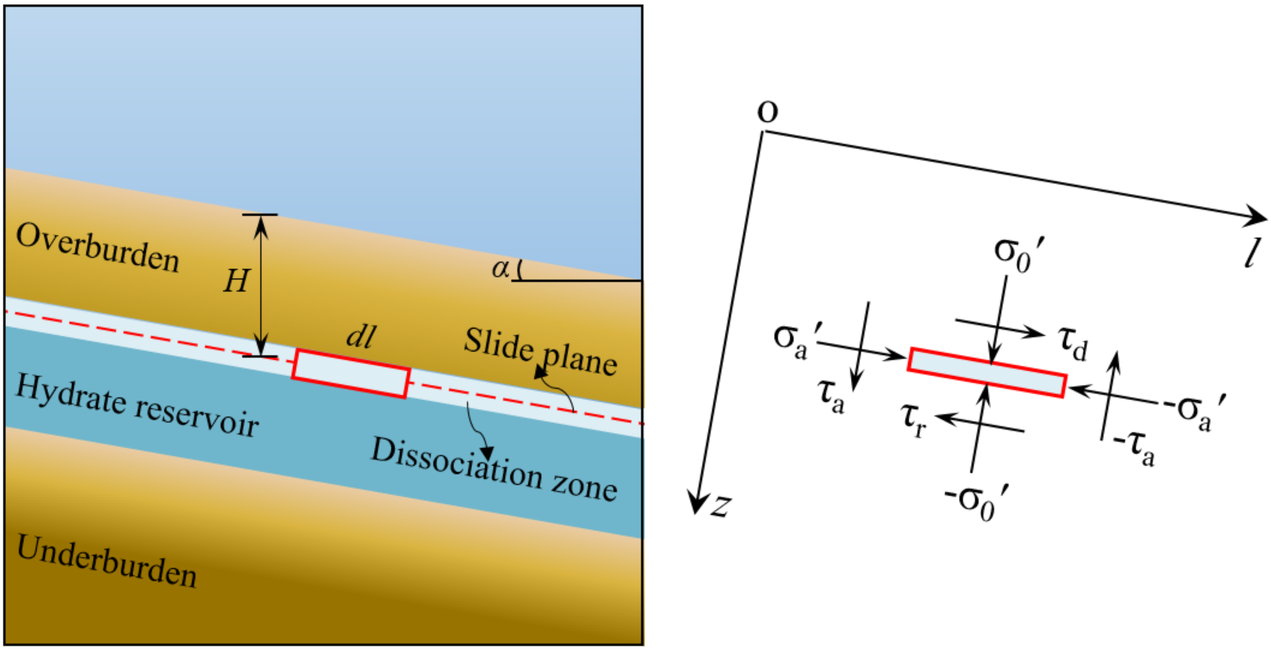

(a) (b)

Fig. 6. (a) Schematic diagram of an infinite submarine slope undergoing hydrate dissociation. (b) The force system acting on the unit slide plane. Note: For illustration, the position of the slide plane in this figure is assumed, and its real position will change with the propagation of the dissociation front of the hydrate reservoir.

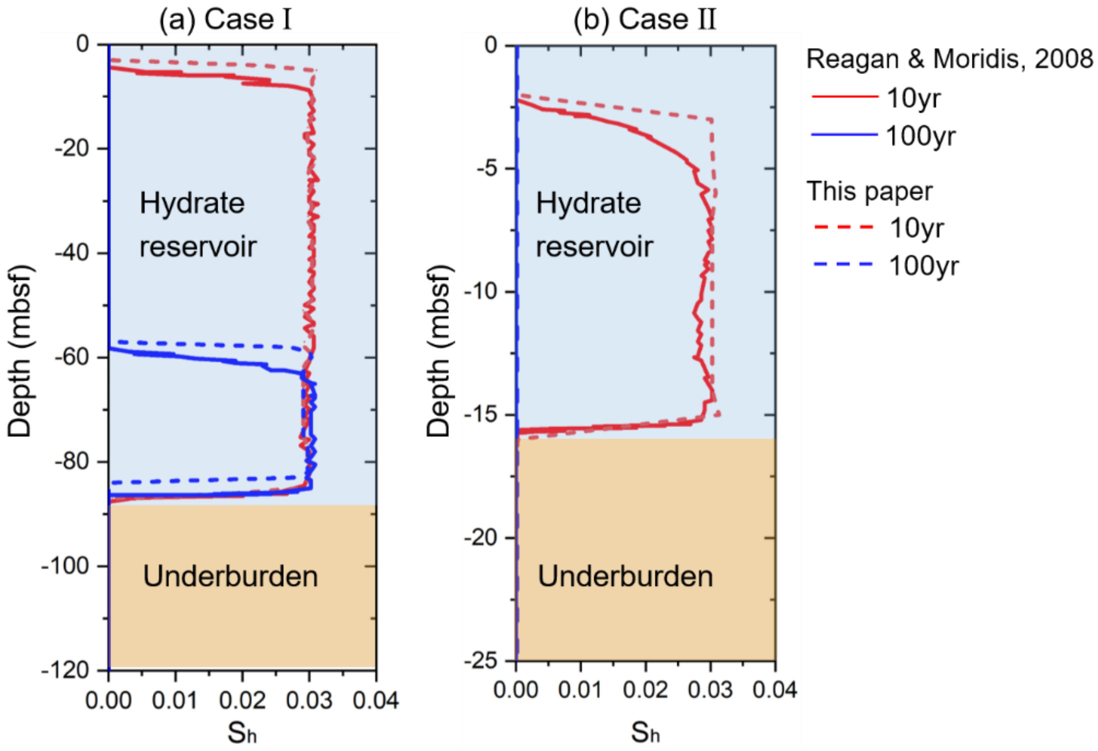

Fig. 7. The evolution of hydrate saturation profiles: (a) Case I: cold, shallow hydrate deposits; (b) Case II: warm, shallow hydrate deposits.

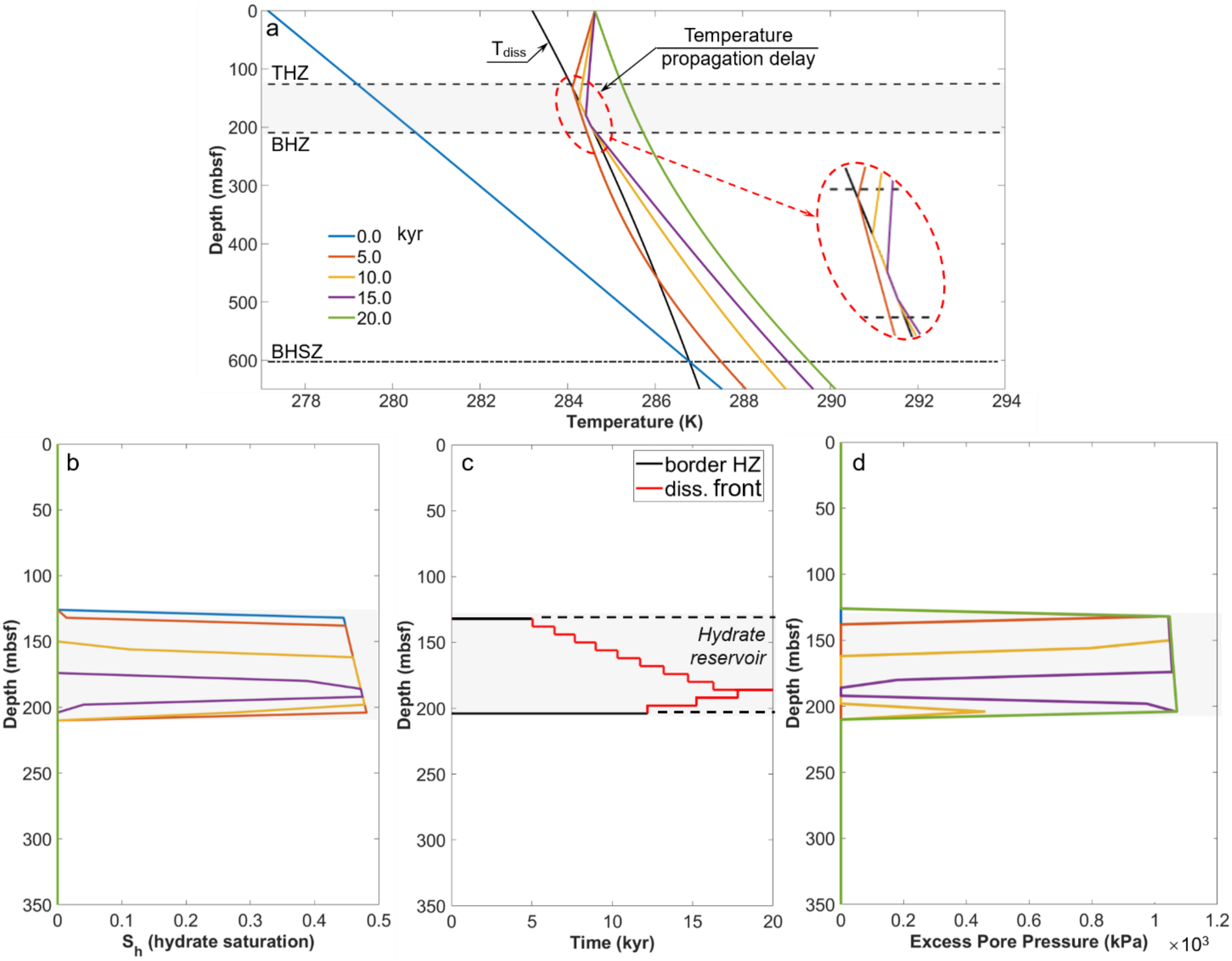

Fig. 8. Evolution of (a) the temperature profile, (b) the hydrate saturation profile, (c) the border and dissociation front of the hydrate zone (HZ), and (d) the excess pore pressure due to a gradual temperature increase at the seafloor caused by climate warming (Case I).

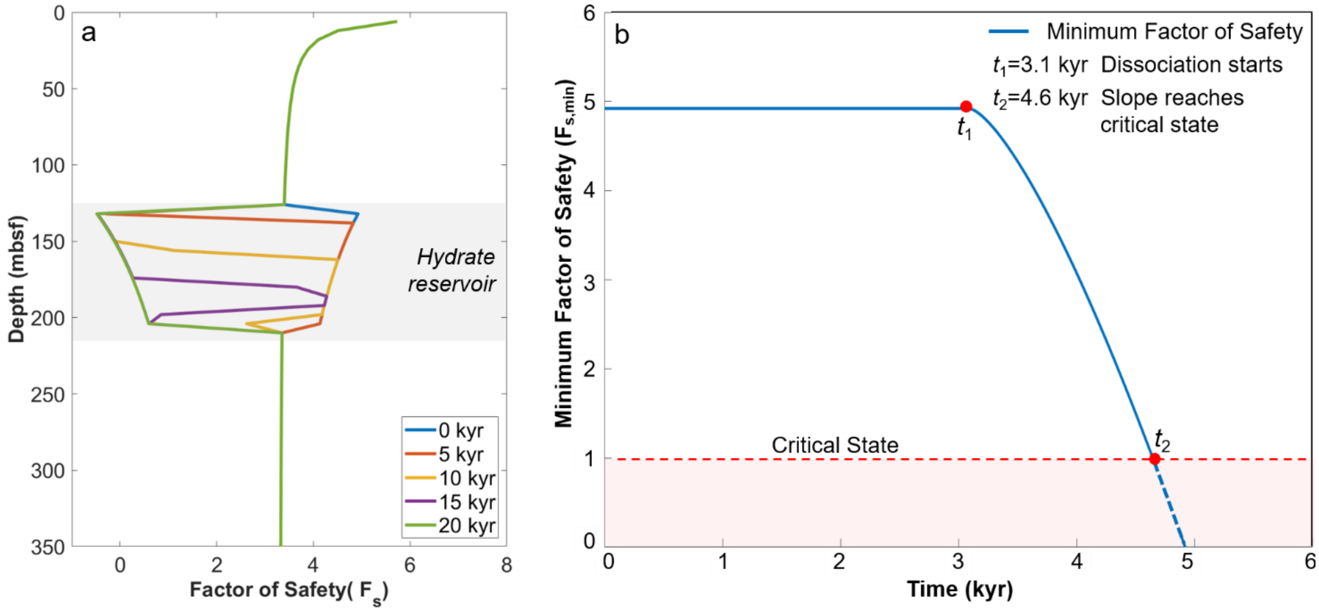

Fig. 9. (a) Evolving profile of slope safety factor variation along depth. (b) The temporal evolution of the minimum factor of slope safety under a gradual temperature increase at the seafloor due to climate warming (Case I).

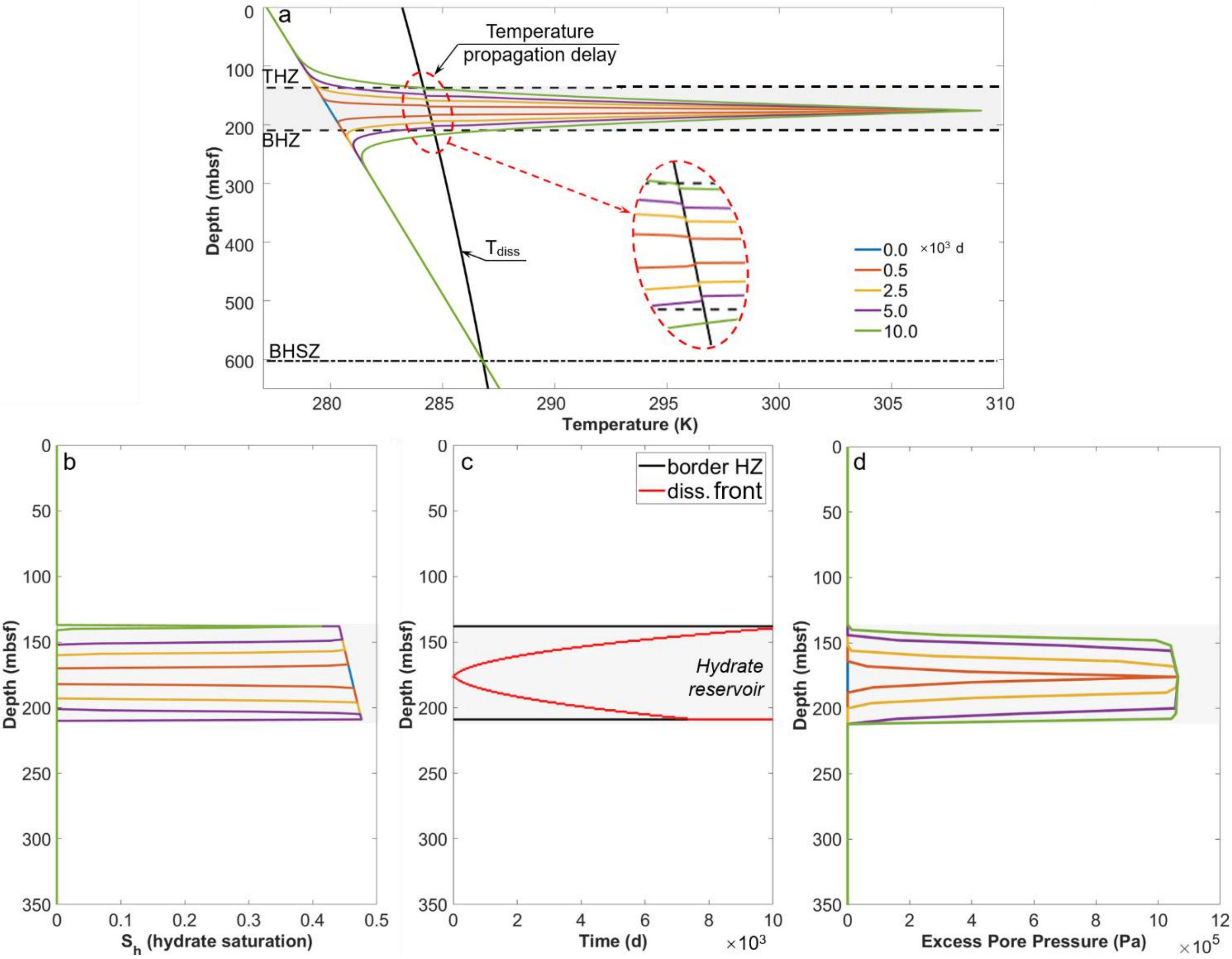

Fig. 10. Evolution of (a) the temperature profile, (b) the hydrate saturation profile, (c) the border and dissociation front of the hydrate zone (HZ), and (d) the excess pore pressure due to a sharp temperature increase inside the hydrate deposit caused by thermal stimulation during hydrate extraction (case II).

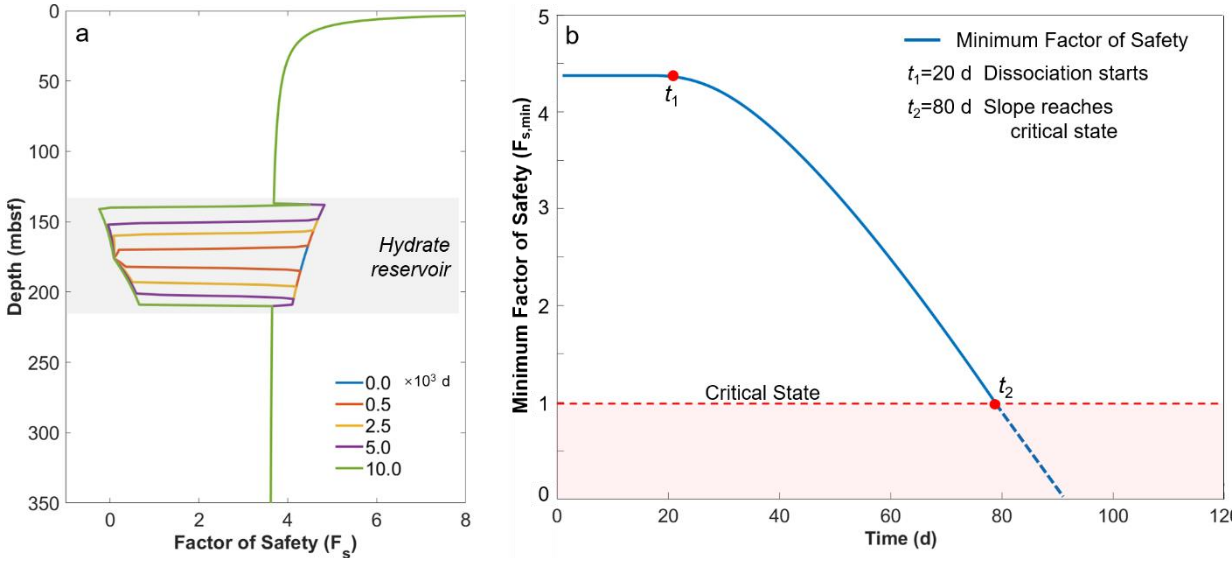

Fig. 11. Temporal evolution of the slope safety factor (a) and the minimum factor of slope safety (b) under a sharp temperature increase inside the hydrate deposit due to hydrate extraction (case II).

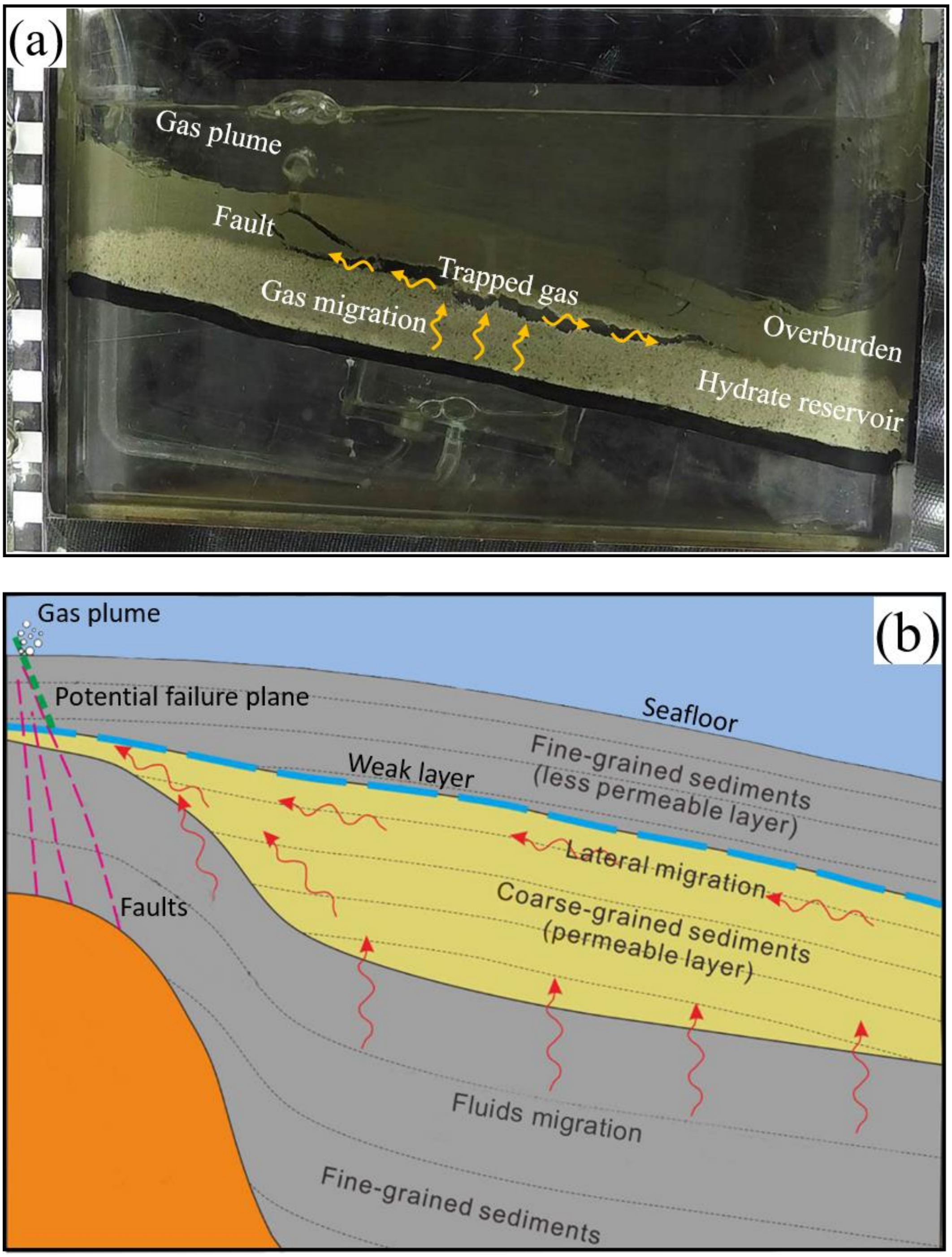

Fig. 12. (a) Disc-shaped failure: a possible hydrate-bearing slope failure pattern under a gradual temperature increase at the seafloor due to climate warming (Nian et al., 2022); (b) schematic illustration of a slope failure case in the northern South China Sea (Sun et al., 2018).

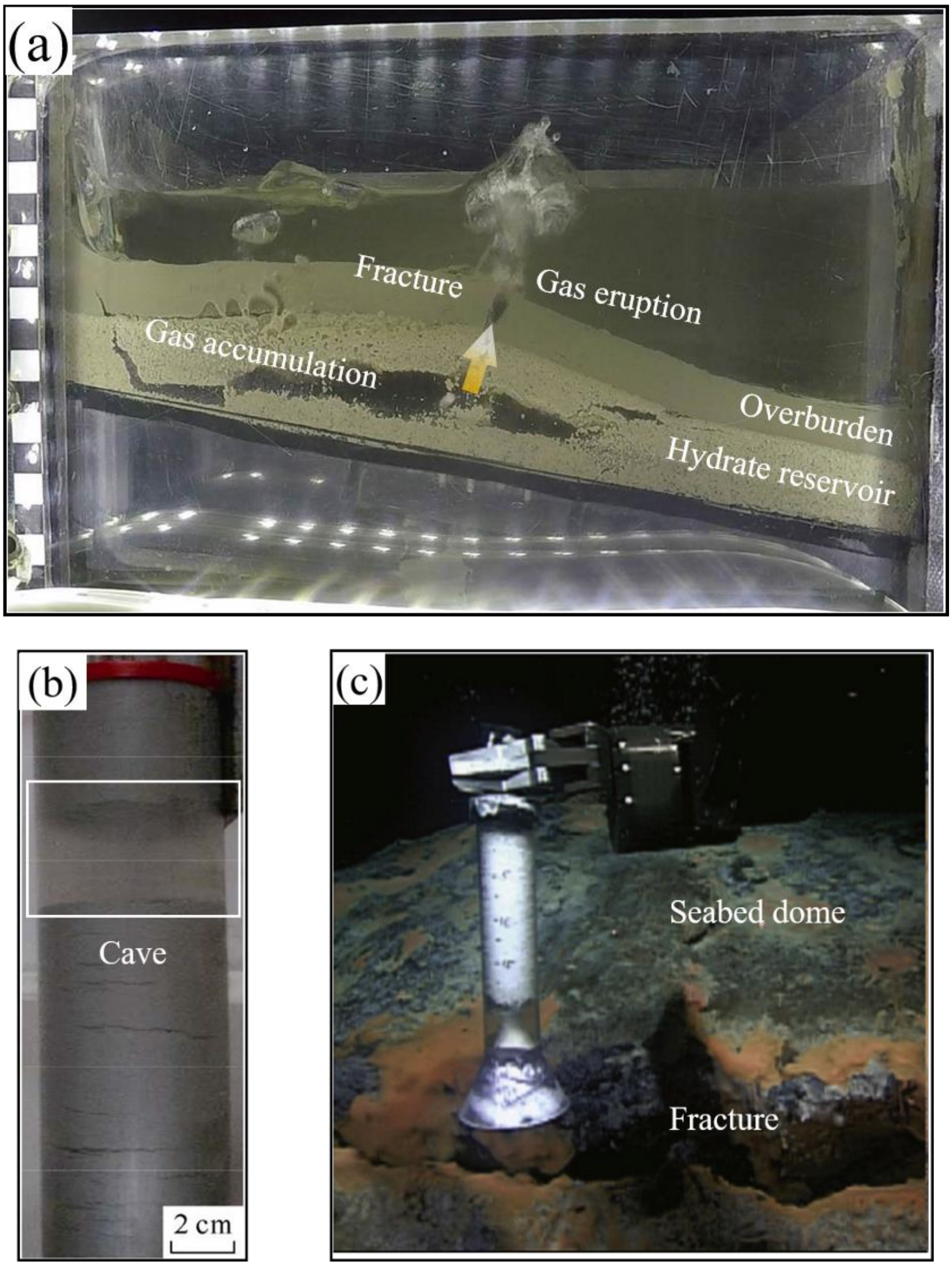

Fig. 13. (a) Penetration failure: a possible hydrate-bearing slope failure under a sharp temperature increase due to hydrate extraction (Nian et al., 2022); (b) cavity structure resulting from the dissociation of gas hydrate in the Shenhu area (Zhang et al., 2017); (c) a crack near the crest of a dome in the Santa Monica Basin, offshore California, from which a continuous plume of gas emanates (modified from Paull et al., 2008).

Table captions

Table 1. Summary of parameters and units used in this study.

Parameter	Definition	Unit	Value
Parameters for Hydrate reservoir			
z	Depth	m	
α	Slope angle	°	3
H_w	Water depth	m	1274
S_h	Initial hydrate saturation	%	46.2
G	Geothermal gradient	K/km	45-67
k	Permeability	m^2	5.5×10^{-15}
S	Salinity	%	3.5
κ	Thermal diffusivity	m^2/s	4.5×10^{-7}
γ'	Buoyant weight	kN/m^3	6.5
ϕ	Porosity	m^3/m^3	0.3
L	Latent heat of melting gas hydrate	J/kg	56552-16.8/T
E_s	Confined compression modulus	mPa	10
c_1'	Initial cohesion	kPa	100
c_2'	Cohesion after hydrate dissociation	kPa	5.5
$\varphi'/$	Internal friction angle	°	8.03
Parameters used to implement the THC coupling model of Xu and Ruppel (1999)			
M_{sl}	Solubility of methane gas in liquid phase	kg/kg	---
q_f	Fluxes of total mass	kg/(m·s)	4×10^{-8}
q_e	Fluxes of energy	W/m^2	0.05
q_m	Flux of methane	kg/(m·s)	6×10^{-11}
λ	Effective thermal conductivity	W/(m·K)	3.66
C_p	Effective isobaric specific heat capacity	J/(kg·K)	---
C_{pl}	Isobaric specific heat capacity of the liquid	J/(kg·K)	4.18×10^3
C_{ph}	Isobaric specific heat capacity of hydrate	J/(kg·K)	2.16×10^3